Supporting Information

Distinct Behaviors of Cu- and Ni-ZSM-5 Zeolites Toward the Post-Activation Reactions of Methane

Muhammad Haris Mahyuddin,*[a,b] Seiya Tanaka,[c] Ryotaro Kitagawa,[c] Arifin Luthfi Maulana,[a] Adhitya Gandaryus Saputro,[a,b] Mohammad Kemal Agusta,[a,b] Hadi Teguh Yudistira,[d] Hermawan Kresno Dipojono,[a,b] and Kazunari Yoshizawa*[e]

[a] Research Group of Advanced Functional Materials, Faculty of Industrial Technology, Institut Teknologi Bandung, Bandung 40132, Indonesia

[b] Research Center for Nanoscience and Nanotechnology, Institut Teknologi Bandung, Bandung 40132, Indonesia

[c] Department of Chemistry and Biochemistry, Graduate School of Engineering, Kyushu University, Fukuoka 819-0395, Japan

[d] Mechanical Engineering Study Program, Institut Teknologi Sumatera, South Lampung 35365, Indonesia

[e] Institute for Materials Chemistry and Engineering and IRCCS, Kyushu University, Fukuoka 819-0395, Japan

* To whom all correspondences should be addressed

(e-mail: haris[at]tf.itb.ac.id and kazunari[at]ms.ifoc.kyushu-u.ac.jp).

Table of Contents:

Section S1. Comparison of energy diagrams calculated by using different U_{eff} values for the Ni 3d orbitals

We show below (Figure S1) a comparison of energy diagrams calculated by using *U* = 4.0 and 6.4 eV for the C–H pathway of the CH_3OH oxidation to CH_2O over the reduced $[Ni^{II}_2(\mu\text{-}O)]^{2+}$ active site. As can be seen from these two energy diagrams, the used of *U* = 4.0 and 6.4 eV results in comparable CH_3OH adsorption energies and the same ground spin state (open-shell singlet state) for the $[Ni_2O]^{2+}$-MFI + CH_3OH and **RC-1** states. However, a discrepancy in the relative energy occurs when the reaction proceeds to **TS-1** and **IC-1**, where the ground state starts changing to the triplet state. Focusing on **IC-1**, we understand that the triplet ground state can be formed either by two Ni^{3+} or two Ni^{+} or a pair of Ni^{3+} and Ni^{+} because only these two Ni oxidation states may have one unpaired electron configuration (see also Scheme S1 below). Since we found in the Cu case (Figure 3a of the revised manuscript) that **IC-1** involves a pair of Cu^{3+} and Cu^{+}, we expect the same also occurs for the Ni case. Thus, to treat correctly the correlation effect of Ni^{3+}, the use of *U* = 4.0 eV is the only option (see our previous work[1] and a comparison of Ni^{3+} spin densities calculated by using *U* = 4.0 and 6.4 eV in Table S1 below).

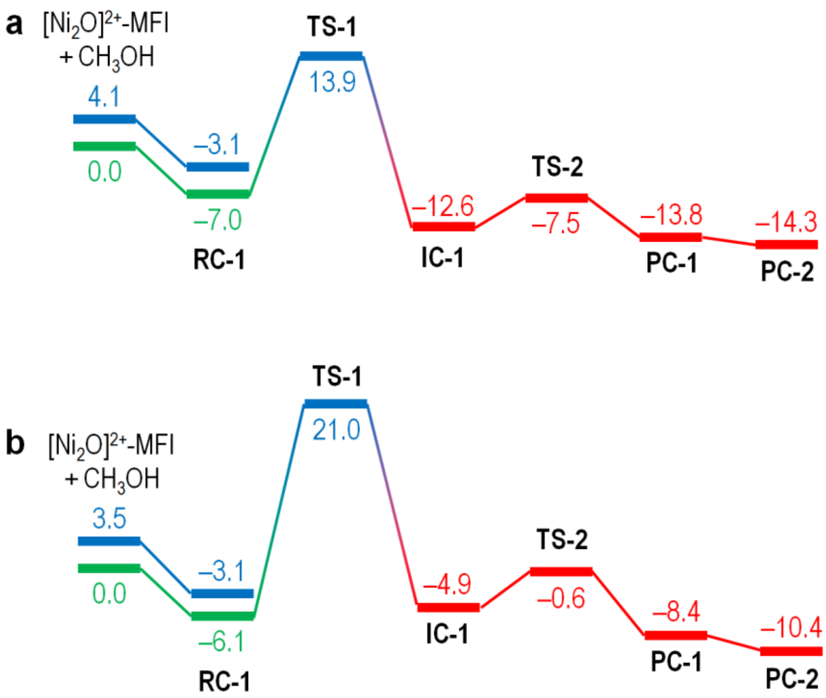

Figure S1. Energy diagrams (in kcal/mol) of the CH_3OH oxidation to CH_2O via the C–H pathway over the $[Cu–O–Cu]^{2+}$ active site calculated by using (a) U = 4.0 eV and (b) U = 6.4 eV. Blue, red, and green lines correspond to the quintet, triplet, and open-shell singlet states, respectively.

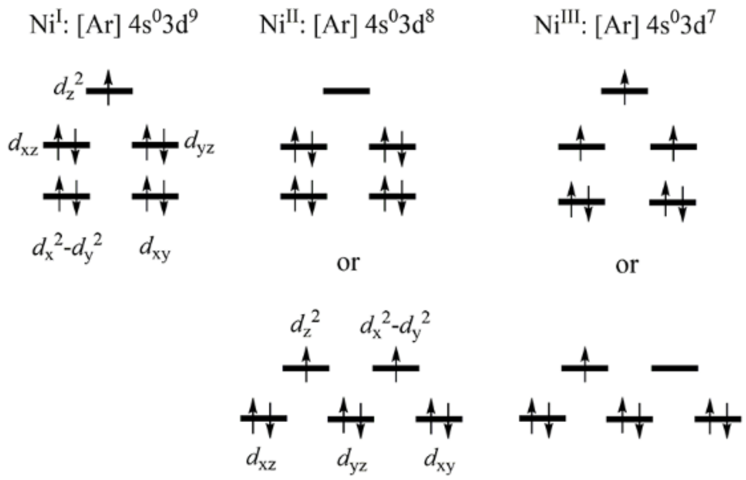

Scheme S1. Possible configurations of the outermost electrons in Ni^{+}, Ni^{2+}, and Ni^{3+} cations, leading to the formation of doublet, singlet or triplet, and quartet or doublet, respectively.

Table S1. Spin density of Ni centers indicating the number of unpaired electrons in the outer shell.

U **(eV)**	**Reaction step**	**Spin state**	ρ**(Ni1, Ni2)**
4.0	RC-1	OSS	1.60, −1.60
	TS-1	Quintet	1.45, 1.44
	IC-1	Triplet	1.09, 1.00
	TS-2	Triplet	1.07, 1.00
	PC-1	Triplet	1.03, 0.96
	PC-2	Triplet	1.05, 1.05
6.4	RC-1	OSS	1.70, −1.70
	TS-1	Quintet	1.54, 1.46
	IC-1	Triplet	1.30, 0.98
	TS-2	Triplet	1.24, .098
	PC-1	Triplet	1.08, 0.97
	PC-2	Triplet	1.02, 1.02

IC-1 involves Ni^{3+} and Ni^{+}, each of which is expected to have spin density (number of unpaired electrons) of one. This can be correctly treated only when U = 4.0 eV is used. When U = 6.4 eV is used, however, one of the Ni centers has a spin density of 1.30, which is incorrect for Ni^{3+}.

Section S2. Computational methods for calculating reaction rate constants

For performing the kinetic simulations to calculate reaction rate constants, we use the transition state theory-based Arrhenius equation, as follow.

$$k_{for} = \frac{k_B T}{h} \frac{Z^{\ddagger}}{Z} \exp\left(-\frac{E_a}{RT}\right) \approx \frac{k_B T}{h} \exp\left(-\frac{E_a}{RT}\right)$$

where E_a is the activation barrier, k_B is the Boltzmann constant, h is the Planck constant, R is the universal gas constant, and T is the variating reaction temperature. We previously found that the partition function ratio $(Z^{\ddagger}/Z)$ for surface-bound reactions is approximately close to unity.[2]

Table S2. Geometrical parameters along the hydrolysis of CH_3 ligand to CH_3OH over partially reduced Cu-ZSM-5 in the closed-shell singlet state.

Reaction step	$d_{C\text{–}OF}$ (Å)	$d_{C\text{–}Cu1}$ (Å)	$d_{C\text{–}Ow}$ (Å)	$d_{H\text{–}Ow}$ (Å)	$d_{H\text{–}Oa}$ (Å)	$d_{Cu\text{–}Ow}$ (Å)	$d_{Cu\text{–}Oa}$ (Å)
RC-1	1.51	3.25	3.35	0.99	1.80	3.59, 4.10	1.87, 1.90
TS-1	1.49	3.24	3.44	1.02	1.62	2.06, 3.25	2.30, 1.84
IC-1	1.49	3.32	4.04	1.43	1.07	1.84	1.89
TS-2	2.15	2.60	3.57	2.58	0.98	1.84, 1.94	2.35
IC-2	3.09	1.96	2.79	3.43	0.98	1.82, 1.91	2.10
TS-3	3.52	2.27	2.03	3.27	0.98	1.85, 2.02	2.10
PC-1	4.44	2.96	1.47	3.30	0.98	1.91	1.94

O_w and O_a denote the O atom of the H_2O and Cu–O–Cu, respectively.

Table S3. Geometrical parameters along the oxidation of CH_3 ligand to C_2H_6O over partially reduced Cu-ZSM-5 in the closed-shell singlet state.

Reaction step	$d_{C–OF}$ (Å)	$d_{C1–Om}$ (Å)	$d_{H–Om}$ (Å)	$d_{H–Oa}$ (Å)	$d_{Cu–Om}$ (Å)	$d_{Cu–Oa}$ (Å)
RC-2	1.50	3.19	0.98	1.93	2.95, 3.94	1.88, 1.90
TS-4	1.50	3.30	1.03	1.55	2.02, 3.43	2.40, 1.84
IC-3	1.50	3.29	1.44	1.07	1.85	1.92
TS-5	2.13	2.96	1.42	1.07	1.85	1.90
PC-2	3.54	1.46	2.53	0.98	1.94	1.96

O_m and O_a denote the O atom of the CH_3OH and Cu–O–Cu, respectively. C1 denotes the C atom of the CH_3O_F.

Table S4. Geometrical parameters and atomic spin densities (ρ) along the C–H pathway of CH_3OH oxidation to CH_2O on fully reduced Cu–O_2–Cu and Ni–O_2–Ni active sites.

Catalyst	Reaction step	Ground state [a]	d_{M-C} (Å)	d_{M-O} (Å)	d_{C-H} (Å)	$d_{\mu O-H}$,	d_{O-H} (Å)	d_{C-O} (Å)	ρ(M1, M2)	ρ(μO, O, C)
Cu-ZSM-5	RC-1	Triplet	3.92	3.66	1.10	-	0.97	1.43	0.51, 0.51	0.72, 0.06, 0.00
	TS-1	Triplet	3.27	3.95	1.31	1.29	0.98	1.38	0.40, 0.38	0.48, 0.20, 0.31
	IC-1	CSS	2.07	2.85	2.73	0.97	0.98	1.34	0.00, 0.00	0.00, 0.00, 0.00
	TS-2	CSS	2.10	2.56	-	0.98	1.54	1.26	0.00, 0.00	0.00, 0.00, 0.00
	PC-1	CSS	1.99	1.87	-	0.99	1.76	1.30	0.00, 0.00	0.00, 0.00, 0.00
	PC-2	CSS	-	1.92	-	0.99	3.41	1.26	0.00, 0.00	0.00, 0.00, 0.00
Ni-ZSM-5	RC-1	OSS	4.12	4.19	1.10	-	0.97	1.43	1.60, –1.60	0.00, 0.00, 0.00
	TS-1	Quintet	3.40	4.07	1.39	1.19	0.97	1.38	1.45, 1.44	0.33, 0.19, 0.36
	IC-1	OSS	1.99	2.76	2.72	0.97	0.98	1.36	1.17, –1.08	0.00, –0.04, –0.06
	TS-2	Triplet	1.97	2.10	-	0.98	1.15	1.32	1.07, 1.00	0.04, –0.07, –0.13
	PC-1	Triplet	1.98	1.90	-	0.99	1.78	1.30	1.03, 0.96	0.01, –0.02, –0.08
	PC-2	Triplet	-	1.98	-	0.99	3.05	1.27	1.05, 1.05	0.03, 0.00, –0.02

[a] CSS and OSS stand for closed-shell and open-shell singlet states, respectively.

Table S5. Geometrical parameters and atomic spin densities (ρ) along the (O–H)$_a$ pathway of CH_3OH oxidation to CH_2O on fully reduced Cu–O_2–Cu and Ni–O_2–Ni active sites.

Catalyst	Reaction step	Ground state [a]	$d_{M–C}$ (Å)	$d_{M–O}$ (Å)	$d_{C–H}$ (Å)	$d_{\mu O–H}$,	$d_{O–H}$ (Å)	$d_{C–O}$ (Å)	ρ(M1, M2)	ρ(μO, O, C)
Cu-ZSM-5	RC-2	Triplet	3.80	2.90, 2.66	1.10	-	0.97	1.45	0.53, 0.54	0.72, 0.03, 0.00
	TS-3	Triplet	3.25	2.07, 2.26	1.10	1.38	1.13	1.44	0.54, 0.54	0.50, 0.15, 0.01
	IC-2	Triplet	3.00	1.96, 1.96	1.10	0.98	-	1.43	0.56, 0.56	0.26, 0.31, 0.01
	TS-4	CSS	2.77	2.00, 2.04	1.36	0.98, 1.31	-	1.36	0.00, 0.00	0.00, 0.00, 0.00
	PC-2	CSS	-	1.92	-	0.99, 0.99	-	1.26	0.00, 0.00	0.00, 0.00, 0.00
Ni-ZSM-5	RC-2	OSS	3.40	2.30, 2.26	1.10	-	0.98	1.47	1.65, –1.65	0.01, –0.01, 0.00
	TS-3	OSS	3.43	2.23, 2.10	1.10	1.39	1.13	1.44	1.653 –1.63	0.01, –0.01, 0.00
	IC-2	Quintet	2.90	1.96, 1.96	1.10	0.97	-	1.44	1.72, 172	0.00, 0.18, 0.01
	TS-4	Quintet	2.72	2.00, 2.00	1.43	0.98, 1.24	-	1.37	1.43, 1.43	0.21, 0.31, 0.34
	PC-2	Triplet	-	1.98	-	0.99, 0.99	3.05	1.27	1.05, 1.05	0.03, 0.00, –0.02

[a] CSS and OSS stand for closed-shell and open-shell singlet states, respectively.

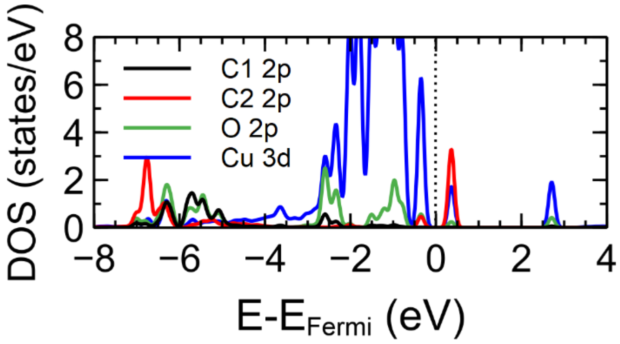

Figure S2. Projected Density of States (PDOS) of TS-5 in the CH_3 oxidation to C_2H_6O on reduced Cu active site.

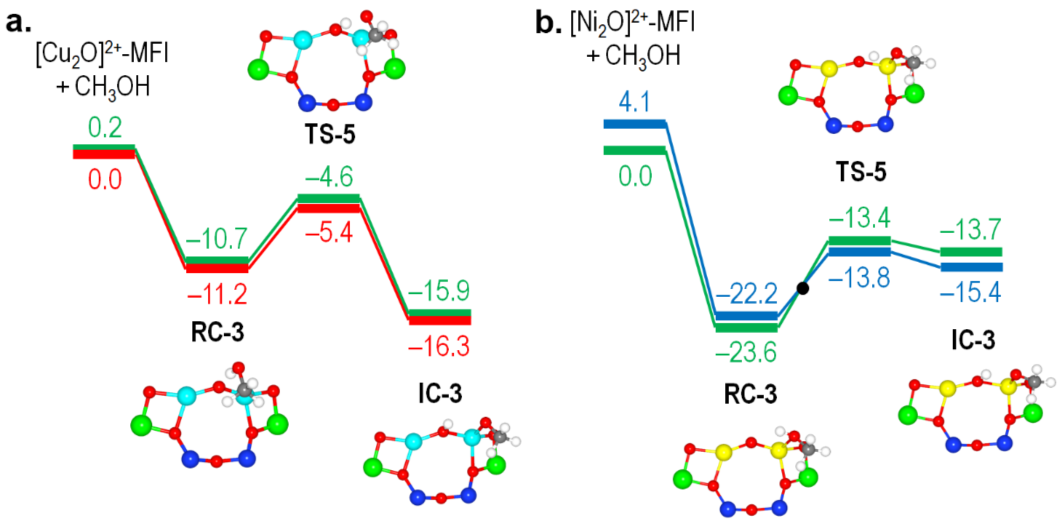

Figure S3. Energy diagrams (in kcal/mol) of CH_3OH oxidation to CH_2O via the $(O–H)_b$ pathway over (a) $[Cu–O–Cu]^{2+}$ and (b) $[Ni–O–Ni]^{2+}$ active sites in the quintet (blue lines), triplet (red lines), and singlet (green lines) states.

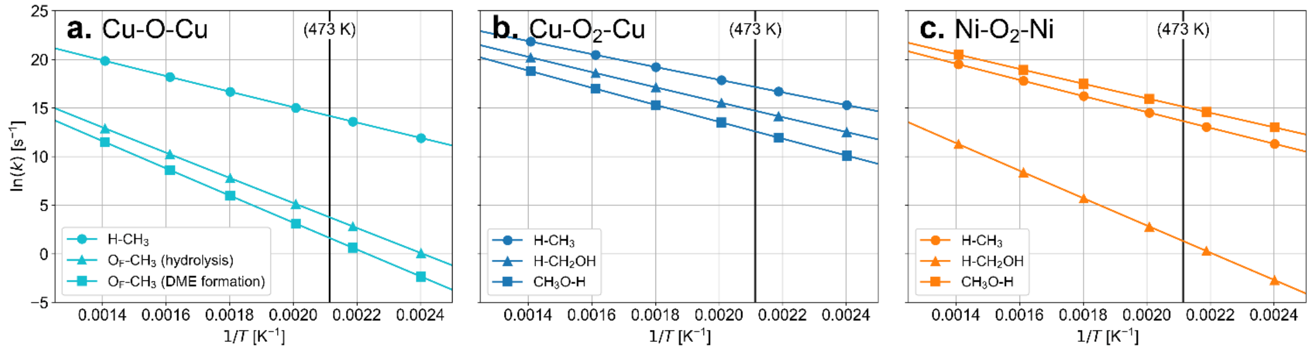

Figure S4. Simulated Arrhenius plots for the rate-determining H–CH_3, O_F–CH_3, H–CH_2OH, and CH_3O–H activation steps over the (a) mono(μ-O)Cu_2, (b) bis(μ-O)Cu_2, and (c) bis(μ-O)Ni_2 active sites.

As shown in Figure S4a, the mono(μ-O)Cu_2 species activates CH_4 at 473 K with a high reaction rate (about 14 s^{-1}), which is ten order of magnitude higher than the formation of CH_3OH via the hydrolysis reaction and C_2H_6O via the dissociative pathway, suggesting that the activated CH_4 (i.e., the surface CH_3) would remain on the zeolite framework and the products (CH_3OH or C_2H_6O) would not come out if there is no solvent (H_2O or CH_3OH) added to the reactor. This, in fact, is consistent with the experimental observations.[3,4]

In Figure S4b, we show that the bis(μ-O)Cu_2 active site, in term of activity toward CH_4, is more superior than the mono(μ-O)Cu_2 active site. This superiority, however, comes with a trade-off for being easy and rapid to over-oxidize the formed CH_3OH, as indicated by the similarity in the reaction rates for the H–CH_3 and H–CH_2OH activation steps at all temperature. This result is actually anticipated to some extent since the reduced Cu–O–Cu species is also highly active toward the CH_4 oxidation.

For the bis(μ-O)Ni_2 active site (Figure S4c), on the other hand, we found a good balance between activities toward CH_4 and CH_3OH. More specifically, the H–CH_3 activation rate is found to be as high as that in the mono(μ-O)Cu_2 case with a very low H–CH_2OH activation rate, suggesting that the easily desorbed CH_3OH can be protected from the overoxidation to CH_2O.

References

1. Mahyuddin, M. H.; Yoshizawa, K. DFT Exploration of Active Site Motifs in Methane Hydroxylation by Ni-ZSM-5 Zeolite. *Catal. Sci. Technol.* **2018**, *8*, 5875–5885.
2. Saputro, A. G.; Putra, R. I. D.; Maulana, A. L.; Karami, M. U.; Pradana, M. R.; Agusta, M. K.; Dipojono, H. K.; Kasai, H. Theoretical Study of CO_2 Hydrogenation to Methanol on Isolated Small Pd_x Clusters. *J. Energy Chem.* 2019, *35*, 79–87.
3. Groothaert, M. H.; Smeets, P. J.; Sels, B. F.; Jacobs, P. A.; Schoonheydt, R. A. Selective Oxidation of Methane by the Bis(μ-Oxo)dicopper Core Stabilized on ZSM-5 and Mordenite Zeolites. *J. Am. Chem. Soc.* **2005**, *127*, 1394–1395.
4. Wulfers, M. J.; Lobo, R. F.; Ipek, B.; Teketel, S. Conversion of Methane to Methanol on Copper-Containing Small-Pore Zeolites and Zeotypes. *Chem. Commun.* **2015**, *51*, 4447–4450.